Journal of Materials Chemistry C

Accepted Manuscript

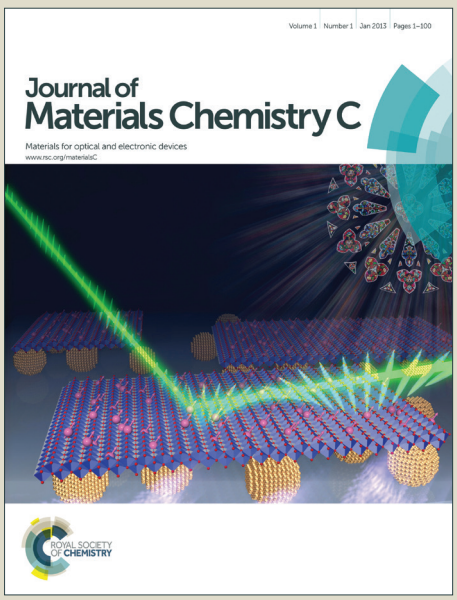

ROYAL SOCIETY OF CHEMISTRY

www.rsc.org/materialsC

Journal of Materials Chemistry C

Cite this: DOI: 10.1039/c0xx00000x

www.rsc.org/xxxxxx

Full Paper

Self-assembly of Pseudorotaxane Films with Thermally Reversible Crystal Phases and Optical Properties

Yaching Tsai,[a] Kai-Jen Chen,[a] Chun-Jen Su,[b] Wei-Ru Wu,[b] U-Ser Jeng[a,b] and Masaki Horie*[a]

Received (in XXX, XXX) Xth XXXXXXXXX 20XX, Accepted Xth XXXXXXXXX 20XX

DOI: 10.1039/b000000x

Highly ordered thin films of a pseudorotaxane consisting of the host cyclic molecule, dibenzo[24]crown-8 (DB24C8), and guest axle molecule *N*-(xylylammonium)-methylferrocene were prepared on solid substrates via solution casting followed by annealing. Collective evidence obtained from X-ray diffraction, differential scanning calorimetry, polarised optical microscopy (POM) and grazing incident wide-angle X-ray scattering (GIWAXS) experiments indicate that the specially architectured host and guest molecules can first form a highly ordered crystalline phase upon solvent evaporation. Annealing of this phase at temperatures above 130 °C leads to an irreversible transition of the crystal phase to a high-temperature (HT) crystalline phase with triclinic crystalline domain sizes of 50–100 μm. When cooled back to room temperature, the HT phase undergoes a solid–solid phase transition to a low-temperature (LT) crystalline phase of a similar triclinic form but favouring a tighter packing of axle molecules. Thermally reversible LT–HT phase transitions were consistently evidenced via in situ observations by POM and X-ray scattering and are attributed to a subtle ordering competition between the host cyclic molecules and guest axle molecules. This local structural transition, however, only slightly affects the stability of the layering frame structure of the pseudorotaxane film; in which the supermolecular complex adopts an edge-on orientation with the cyclic molecular plane being perpendicular to the substrate and is interlocked via interactions with the axle molecules. The results demonstrate the feasibility of self-assembled pseudorotaxane films with thermally driven phase transitions as a possible molecular switch.

[a] *Department of Chemical Engineering, Frontier Research Center on Fundamental and Applied Sciences of Matters, National Tsing Hua University, 101, Sec. 2, Kuang-Fu Road, Hsin-Chu, 30013 Taiwan; E-mail: mhorie@mx.nthu.edu.tw*

[b] *National Synchrotron Radiation Research Center, 101, Hsin-Ann Rd. Science Park, Hsinchu, 30076, Taiwan*

† Electronic Supplementary Information (ESI) available. ^{1}H NMR spectra, DSC charts and 2D GIWAXS patterns. See DOI: 10.1039/b000000x/

Introduction

The synthesis of mechanically interlocked molecules such as rotaxanes[1,2] and catenanes[3,4] have been intensively studied for their controlled molecular structures in solutions. To achieve higher order molecular movements, rotaxane films[5,6], molecular gyroscopes[7] and metal–organic frameworks (MOFs)[8,9] have been developed and designed to allow molecular movement in the solid state. In this context, film formation with controlled morphology is indispensable for the fabrication of optoelectronic devices. Samorì and his colleagues reported the drop-casting and solvent vapour annealing (SVA) treatment[10,11] of organic functional molecules. In a film of dithiophene rotaxane with *β*-cyclodextrin encapsulation on a gold substrate, rotaxane initially associated into aggregates with limited molecular order when the assembled rotaxane fibre was formed upon SVA treatment.[12] Tanaka and his colleagues reported a triple-decker compound with alkyl chain-substituted porphyrin complexes arranged in a monolayer array on a Au (111) substrate, where the film was deposited via a pulse-injection deposition method.[13] They observed reversible flip-flop rotations induced by a small perturbation from a scanning tunnelling microscope. Although some reports on the self-assembly of supermolecules at the nanoscale have appeared in the literature, only a few groups have demonstrated reversible and modulated complexation and organisation of the supermolecules at the microscale; furthermore, the assembly process and mechanism of pseudorotaxane, which may dissociate to the unthreaded molecules in solution at the nanoscale, has rarely been discussed.

This study focuses on the preparation and order–order structural transitions of thin films of pseudorotaxane [F·DB24C8](PF_6) consisting of *N*-(xylylammonium)-methylferrocene ($[F\text{-}H]^+(PF_6)^-$) and DB24C8 as the axle and cyclic component molecules, respectively.[14] The pseudorotaxane films were deposited on glass substrates from a chloroform solution of this compound by the solvent casting method. Because of the absence of a bulky end group on the pseudorotaxane, the solution process for depositing pseudorotaxane inherently involves an equilibrated state between

the association and dissociation states (Scheme 1, top); therefore, estimation of the complexation ratio of pseudorotaxane in the film state is important. In addition, single crystals of the pseudorotaxane exhibit the ability to undergo a thermally induced phase transition (Scheme 1, bottom). A pair of pseudorotaxanes exhibit intermolecular π–π stacking between the tolyl end groups of the axle component in a unit cell at room temperature. Heating of the crystals induces simultaneous rotations of the aromatic rings of the two axle component molecules, in which the tolyl ends incline to the aromatic plane of the DB24C8. These thermally activated phase-transition features of pseudorotaxane in the form of thin films were examined in parallel by polarised optical microscopy (POM), powder X-ray diffraction (XRD) and grazing incident wide-angle X-ray scattering (GIWAXS).

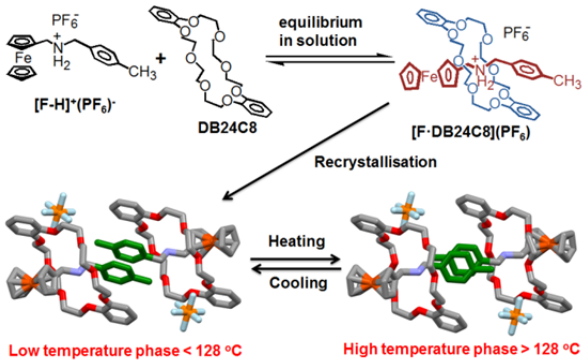

Scheme 1 Synthesis of pseudorotaxane [F·DB24C8](PF_6) and thermally induced molecular motions in solid state.

Experimental section

General methods

DB24C8 was purchased from Sigma-Aldrich. ^{1}H NMR spectra were obtained using a Bruker 500 MHz spectrometer. Pseudorotaxane was synthesized by established procedures.[14] Crystallographic data have been deposited at the CCDC and copies can be obtained on request, free of charge, by quoting the publication citation[14c] and the deposition numbers, 235382, 257706, 257707, and 903277 - 903280. DSC was recorded by Perkin Elmer Diamond DSC. A faster scan rate of 5 °C min^{-1} was used for the DSC measurement (Figure S2) for an improved DSC curve with the sample thin film of small heat flux. XRD patterns were recorded by Brüker D8 SSS diffractometer using CuKα1 (1.54060 Å) irradiation over a 2-theta range of 10 – 50°, with a step size of 0.02 and a time of 2 °C min^{-1}, and the signals were collected by a VANTEC-2000 area detector. The thermo-optical properties of the pseudorotaxane films were observed in polarizing microscope (Olympus BX51-P) with temperature control by the combination of central processor and hot stage (LINKAM TMS92 and THMS600). The monochromic light was generated by using colour filter (Olympus 43IF550-W45).

Film preparation

Thin-films were prepared from a solution of pseudorotaxane [F·DB24C8](PF_6). The molecular structure of pseudorotaxane was confirmed by X-ray single crystallography.[14b,14c] The glass substrates (1 x 1 cm^2) were cleaned with water and acetone in ultrasonic bath for 20 minutes, respectively. 25 mg of fine crystals of pseudorotaxane were dissolved in 1.0 ml chloroform solution, and the solution (100 µl) was then dropped on the glass substrate with a cover of Petri dish to facilitate molecular organization on the substrate surface. After slow evaporation of chloroform in atmosphere at room temperature, an as-grown polycrystalline film with thickness of 6 ± 1 µm was obtained. In order to study solvent effects on the complexation ratio, similar films were also prepared from an acetonitrile solution of pseudorotaxane (25 mg in 1.0 ml acetonitrile). To better understand the initial crystal growth on substrates, a thinner film (3 ± 2 µm) was also prepared from a diluted chloroform solution of pseudorotaxane (25 mg in 2.0 ml chloroform).

GIWAXS measurements

GIWAXS measurements were conducted at the 23A SWAXS end station of the National Synchrotron Radiation Research Center, Taiwan. Details of the instrument were reported in the literature.[15] With an 8 keV (wavelength λ = 1.55 Å) beam and an incident angle 0.2°, time-resolved GIWAXS patterns were collected using a Hamamatsu Flat panel 2D detector, C9728DK, situated 140 mm from the sample position. The scattering wave vector, defined as $q = 4\pi\lambda^{-1}\sin\theta$ (with 2θ the scattering angle), was calibrated using silver behenate.

Results and discussion

Complexation of pseudorotaxane

When crystals of pseudorotaxane were dissolved in chloroform, the ring molecules may thread out with equilibrium constant K_a because the pseudorotaxanes lack a bulky group to prohibit the ring from threading out. The greater complexation ratio in the ^{1}H NMR spectrum of the pseudorotaxanes in chloroform solution (Fig. S1) reveals that chloroform would be a suitable solvent for film casting. For comparison, films were also cast from an acetonitrile solution containing 25 mg of pseudorotaxane in 1.0 ml. Here we compare the diffraction patterns of the films cast by chloroform and acetonitrile solutions of [F·DB24C8](PF_6) (Fig. 1). Despite the cast-film having been prepared from an equilibrated chloroform solution of pseudorotaxane, the observed diffraction peaks match well with those observed for the corresponding single crystals, which confirms that the film primarily contains [F·DB24C8](PF_6) (Figs. 1c and 1d). These results also confirm that the film was free of aggregates of individual components (Figs. 1a and 1b). In contrast, the powder XRD pattern of the acetonitrile-casted film shows weak peaks between 20º and 30º. These peaks can be explained by the lower complexation ratio of pseudorotaxane in the acetonitrile solution than that in the chloroform solution; the acetonitrile solution results in a less crystalline film with poor alignment of the pseudorotaxane salt. The main peaks for these two cases are found at the same diffraction angles (2θ = 16.3° and 19.1°) and are assigned to Miller indexes (01−3) and (122) on the basis of the single-crystal X-ray analysis of pseudorotaxane previously performed. Even though the film prepared from the acetonitrile solution shows poor ordering and crystallinity, the film contains only [F·DB24C8](PF_6) salt. Presumably, this composition is because of the strong self-assembly properties of pseudorotaxane caused by hydrogen bonds between the oxygen atoms of DB24C8 and ammonium cation or methylene protons of the axle group

Table 1 *d*-Spacings calculated from X-ray single-crystal data and XRD patterns of a film.

Miller indexes	from single-crystal X-ray data				from XRD patterns			
	d-spacing (Å)		differential of *d*-spacing (Å)		*d*-spacing (Å)		differential of *d*-spacing (Å)	
	30 °C	128 °C	heating	cooling	30 °C	128 °C	heating	cooling
(122)	4.61	4.73	+0.12	−0.12	4.63	4.71	+0.08	−0.08
(121)	4.91	5.15	+0.24	−0.24	4.88	5.18	+0.30	−0.30
(01−3)	5.43	5.31	−0.12	+0.12	5.40	5.33	−0.07	+0.07

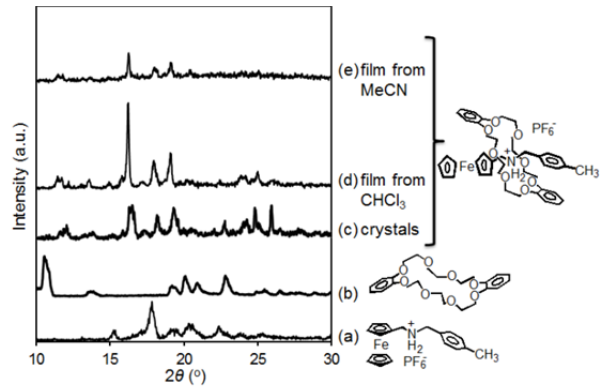

Fig. 1 Powder XRD patterns of (a) axle molecule $[F\text{-}H^+](PF_6)^-$, (b) ring molecule DB24C8, (c) complex [F·DB24C8](PF_6) and the films prepared from (d) chloroform and (e) acetonitrile solutions of [F·DB24C8](PF_6).

and by the intermolecular π–π stacking between two tolyl rings of the neighbouring pseudorotaxanes and intramolecular π–π stacking between the catechol ring and tolyl ring. In the subsequent sections, we primarily discuss the chloroform-cast pseudorotaxane films. The thermal properties of the solution-cast film were measured by differential scanning calorimetry (DSC) to confirm complexation of pseudorotaxane in the films (Fig. S2). The DSC trace of the scratched material shows reversible endothermic and exothermic peaks at 124 and 115 °C, respectively, which is consistent with the DSC results for the fine crystals of [F·DB24C8](PF_6). The DSC scan of the solution-cast sample was substantially different from that of DB28C8, which further supports our hypotheses that the solution cast-film contains [F·DB24C8](PF_6) molecules only and that the reversible peaks are derived from the crystal–crystal phase transition.

X-ray structural analysis

The XRD results for the [F·DB24C8](PF_6) film were isothermally collected at various temperatures thrice. Fig. 2 (a) shows XRD patterns of the [F·DB24C8](PF_6) film at 30°C and 130 °C, and the same film subsequently cooled back to 30 °C. The pattern obtained at 130 °C shows different peaks compared with that obtained at 30 °C, which indicates a change in the molecular structure of [F·DB24C8](PF_6). When the sample was cooled back to 30 °C, the XRD pattern exactly matched the original pattern, suggesting that the molecular structural changes are reversible even in the polycrystalline film. To analyse the evolution of the diffraction peaks upon heating and cooling, we calculated differential patterns and net intensity values (I_{net}), as shown in Fig. 2 (b). In this calculation, the diffraction intensity at 130 °C (I_{130}) was subtracted from that at 30 °C (I_{30}) to give the change in the patterns induced by heating. Similarly, the intensity at 30 °C (I_{30}) was subtracted from that at 130 °C (I_{130}), which afforded the change induced by cooling. In these differential patterns, the peaks between 2θ = 15° and 20° show substantial changes. The peaks corresponding to (121) and (122), which were determined from the computational calculation of single-crystal data, decrease in intensity, and the peak corresponding to (01−3) increases in intensity in the pattern obtained at 130 °C. In addition, the differential XRD pattern obtained by subtracting the patterns obtained after the sample was heated and then cooled mirrors that obtained after the sample was cooled and then heated, indicating excellent reversibility of the thermally activated phase transition of pseudorotaxane even in the polycrystalline film. A detailed comparison is presented in Table 1. The results of this table show that the changes in the *d*-spacing obtained from powder XRD patterns of [F·DB24C8](PF_6) films are consistent with those obtained from the single-crystal X-ray data: the (122) and (121) reflections indicate increases in *d*-spacing of 0.08 and 0.30 Å, respectively, upon heating, whereas the (01−3) reflection indicates an increase in *d*-spacing of 0.07 Å upon cooling.

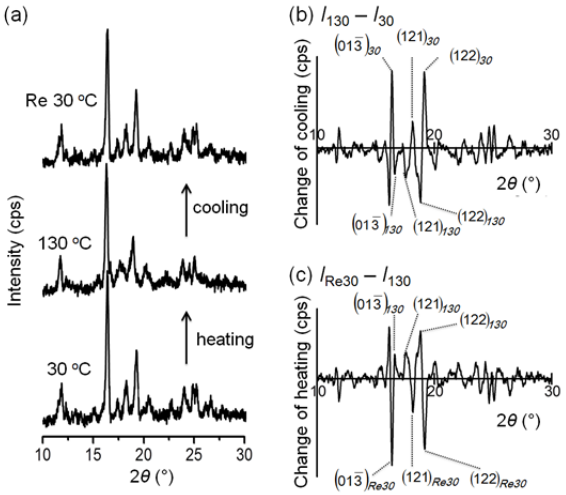

Fig. 2 (a) XRD patterns of the [F·DB24C8](PF_6) film at 30 °C, 130 °C and after cooling back 30 °C. Differential XRD patterns of [F·DB24C8](PF_6) film on (b) heating ($I_{net} = I_{130} - I_{30}$) and (c) cooling ($I_{net} = I_{Re30} - I_{130}$). The Miller indexes were determined by the computational calculation of the single-crystal data.

Fig. 3 reveals the reversible molecular structural change related to the dimensional change of *d*-spacing projected from perpendicular directions to the (122), (121) and (01−3) planes, respectively. The X-ray results show that the lengthened *b*-axis and shortened *a*-axis at the phase-transition temperature (128 °C) are attributable to the anion shift and approach of two catechol groups in ring molecules.[14b,14c] In Figs. 3a and 3b, the expanded (122) and (121) planes are close to the molecular expansion direction caused by the twist of tolyl groups of the axle molecules.

In contrast, the shrunk plane (01−3) is close to an intramolecular shrinkage direction, in which two catechol rings in DB24C8 approach each other as a result of the twist of the axle group. Consequently, the decrease in the *d*-spacing for (01−3) upon phase transition is mainly caused by a shrunken spacing between two catechol rings; i.e. the peak shift corresponding to (01−3) at 130 °C observed from the XRD pattern of [F·DB24C8](PF_6) film is caused, in part, by a tightened packing of the macrocycle molecules.

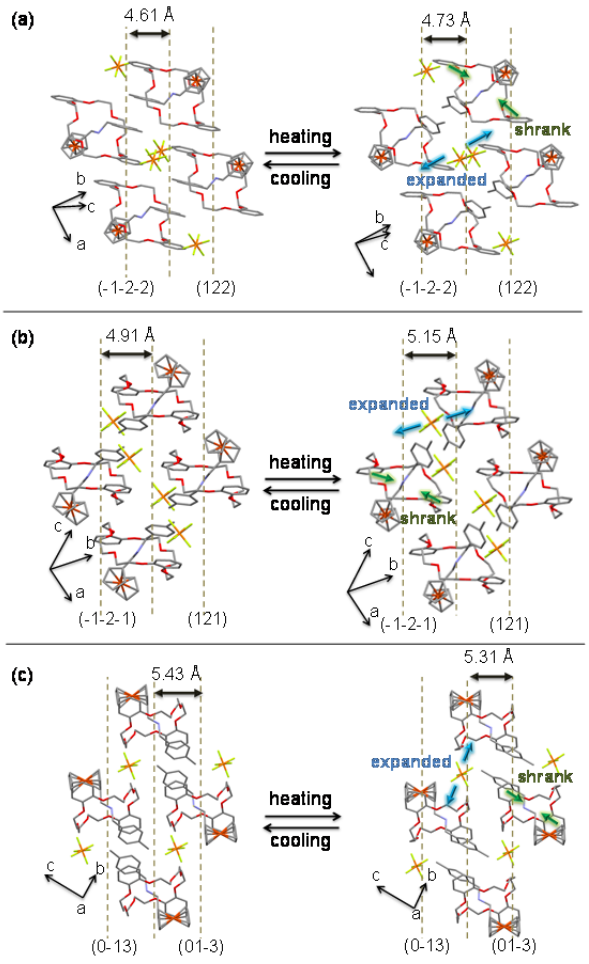

Fig. 3 Illustration of the molecular packing structures of [F·DB24C8](PF_6) at 30 °C and 128 °C from the direction perpendicular to (a) (122), (b) (121) and (c) (01−3). These planes are depicted as dashed lines. Arrows are superimposed to indicate the changed direction at 128 °C.

Thermo-optical properties

The single-crystal X-ray data for pseudorotaxane show that the phase transition of a single crystal causes a twist in the tolyl group of the axle compound, accompanied by the formation of a C–H···π interaction between the tolyl and catechol groups; in contrast, the aromatic planes of DB24C8 are aligned parallel to each other at both 30 °C and 128 °C. This phase transition is responsible for the reversible optical properties of the single crystals of pseudorotaxane, such as light absorption and birefringence, observed by POM.[14b,14c] With an optical compensator, the polarised optical microscope revealed the birefringence of the anisotropic single crystal from the optical retardation value deduced from the interference colour divided by the thickness of the crystal. We conducted temperature-dependent POM observations for solution-cast pseudorotaxane of two different film thicknesses. As shown in Fig. 4a, the POM images of the thicker film (6 ± 1 μm) show multiple interference colours, revealing large amounts of largely randomly oriented crystalline domains at the mesoscale due to uncontrolled crystal growth. The consequent rough film surface may be derived from a heterogeneous solvent evaporation process. The interference colour changed at the phase-transition temperature of approximately 130 °C. Cooling of the film to 30 °C restored the interference colour. These transitions occurred gradually in the film, whereas a single crystal of [F·DB24C8](PF_6) showed an instant interference colour change in less than 70 ms. This gradual colour change is attributed to inhomogeneous heating in the film with a low heat-transfer efficiency because of the nature of polycrystalline grains. Nevertheless, the reversible crystal–crystal phase transitions observed by POM were essentially the same as those observed in the polycrystalline film with fine polycrystal grains.

When the film thickness was reduced (3 ± 2 μm) to achieve less overlapped and more uni-oriented crystalline grains, the POM observations of the thinner film showed four-flabellate-shaped grains, as shown in Fig. 4b (top), which are reminiscent of textures observed for smectic and columnar liquid crystals.[16,17] The appearance of the grain cores probably results from the crystal growth of [F·DB24C8](PF_6) from the centre to the peripheral area with the high-order arrangement of the [F·DB24C8](PF_6) molecules on the glass substrate. When heated, the grain started to reorganise on the substrate at 100 °C. At 130 °C, this reorganisation was completed to provide a large face (50 × 100 μm^2) of the crystal on the glass substrate. In addition, the reorganised crystal domains also exercised reversible interference colour changes during the cycle of cooling and heating (Fig. 4b bottom).

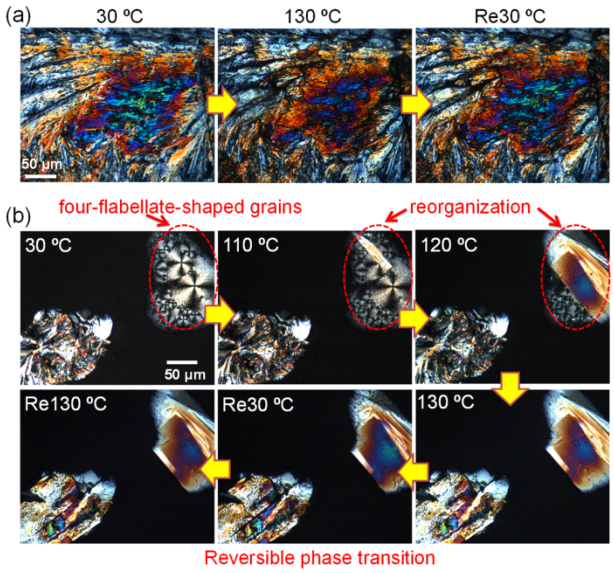

Fig. 4 (a) POM image of a thick film (6 ± 1 μm-thickness) of [F·DB24C8](PF_6) on a glass substrate at 30 °C, 130 °C and after cooling to 30 °C. (b) POM image of a thin film (3 ± 2 μm) of [F·DB24C8](PF_6) on a glass substrate at 30 °C. The film was heated at 110 °C, 120 °C,

130 °C, cooled to 30 °C and then re-heated at 130 °C with a heating/cooling rate of 2 °C min^{-1}. The red-dashed ovals imposed on the photos indicate the reorganisation of pseudorotaxane.

Morphological features revealed with GIWAXS

Morphological features related to the molecular orientation in thin films on solid substrates are difficult to extract from traditional powder XRD data because of the low diffraction intensity of the films and limited observation views (diffraction angles). Therefore, we adopted a synchrotron-based GIWAXS technique with a 2D scattering view in this study.[18,19] By reducing the incident angle on the sample thin film to a fraction of a degree, close to the critical angle of total X-ray reflection of the substrate, we drastically increased the sample path length of the incident X-ray beam and, hence, the diffraction intensity. The setup geometry for GIWAXS and sample orientation are illustrated in Fig. 5, where the vector $q_{\parallel}$ represents the scattering wavevector transfer components parallel to the film surface normal, while q_z represents the same wavevector components perpendicular to the film surface normal. The peaks of the edge-on and face-on Miller indexes {01−1} and {100} are then coincident with the $q_{\parallel}$ and q_z directions, respectively.

The molecular orientation of the thicker (6 ± 1 μm) and thinner (3 ± 2 μm) pseudorotaxane films on silica substrates were observed by 2D GIWAXS (Figs. 5 and S3 in the SI). The 2D GIWAXS patterns for the thicker film exhibit diffraction arcs rather than fine spots, which suggests the existence of crystal domains with considerable orientations (Fig. S3). Nevertheless, the 2D GIWAXS patterns obtained with rotations of the film along the *z*-axis are similar, suggesting that the crystalline grains are relatively uniaxially oriented along the vertical direction but random in the in-plane orientation. In contrast, the thinner film shows relatively fine reflection spots of highly oriented crystal grains in both the normal-to-plane (q_z) and off-normal-plane directions (Fig. 5). Consequently, the GIWAXS patterns observed are sensitive to sample rotation along the *z*-axis, revealing relatively better oriented crystalline grains (see the SI) compared with that in the thicker film. These results are reasonable because the thicker polycrystalline film tends to have more and overlapped crystal domains; therefore, they are easily multi-oriented, as also revealed in the corresponding POM image shown in Fig. 4a. In a thinner film, the pseudorotaxane molecule can exhibit a better synchronised crystal orientation, as shown in Figs. 4b and S3b.

In the following section, we focus on the GIWAXS results for the thinner film (3 ± 2 μm), whose crystal domains are better oriented. According to the X-ray crystallography results for the triclinic single crystals of pseudorotaxane reported previously,[14] the reflection peaks at q = 3.42 nm^{-1} (d = 18.48 Å), q = 4.58 nm^{-1} (d = 13.72 Å), q = 6.76 nm^{-1} (d = 9.29 Å, with respect to $d_{(01-1)}$) and q = 13.39 nm^{-1} (d = 4.69 Å, with respect to $d_{(02-2)}$) shown in the out-of-plane direction are assigned to the {01−1} face of the single crystal, and they are all parallel to the *a*-axis of the unit cell of the crystal. However, the reflections in the off-normal direction at q = 6.26, 6.72, 8.30 and 8.63 nm^{-1} are assigned to the (100), (002), (111) and (1−11) planes, respectively. These planes are all tilted from the (01−1) face: (01−1) < (100) = 84.13°, (01−1) < (002) = 57.76°, (01−1) < (111) = 63.12° and (01−1) < (1−11) = 82.75°. These assignments are summarised in a schematic that allows elucidation of the orientation of the pseudorotaxane molecules on the SiO_2 substrate. As shown in Fig. 5, the pseudorotaxane molecules were anchored on the SiO_2 substrate with the (01−1) plane via the oligo-ethylene glycol group $(CH_2CH_2O)_n$ of DB24C8 of the pseudorotaxane film of an edge-on orientation of the crown ether. This molecular alignment on the substrate is probably due to the molecule–surface (attractive) interactions between oxygen atoms of the crown ether and SiO_2 surface at the earlier stage of crystal growth. Previously, Hosokai et al. also reported a face-on orientation of dibenzo-18-crown-6 on graphite, which they observed by ultraviolet photoelectron spectroscopy and metastable atom electron spectroscopy.[20] In our case, only one side of the crown ether is available for the molecule–surface interaction because of the presence of the bulky axle group. Supermolecular self-assembly of pseudorotaxane leads to the formation of a discotic crystalline phase (refer to the schematic in Fig. 8 below). Presumably, the discotic domains of pseudorotaxane anchor to the substrate with their protruded crown ethers (like feet of centipedes), resulting in the observed edge-on orientation.

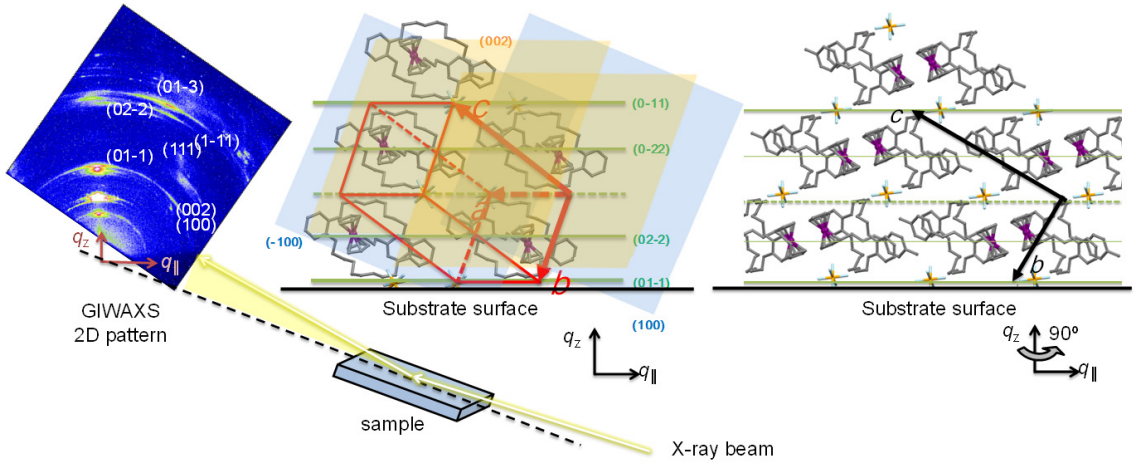

Fig. 5 Schematics for the GIWAXS setup and corresponding sample orientation on the SiO_2 substrate. Related Miller indexes are denoted for the molecular structure.

The structural transformations of the pseudorotaxane film deposited via solution casting were evidenced by in situ GIWAXS during a heating process with a heating rate at 2 °C min^{-1} to 130 °C followed by ambient cooling to 30 °C. Heating of the film caused obvious changes in the 2D GIWAXS patterns, as selectively marked in Fig. 6. In particular, off-normal scattering (01−3) was substantially suppressed, corresponding to the shrinkage of two catechol rings in the high-temperature (HT) crystal phase shown in Fig. 3c. Cooling of the sample film to 30 °C resulted in a slightly modulated GIWAXS pattern corresponding to a low-temperature (LT) crystal phase, as detailed below; i.e. the GIWAXS results provided evidence of structural transitions from the crystalline phase for the as-cast film to the HT phase and then to the LT phase of the pseudorotaxane film, whose transitions were similarly revealed via the previously discussed POM results.

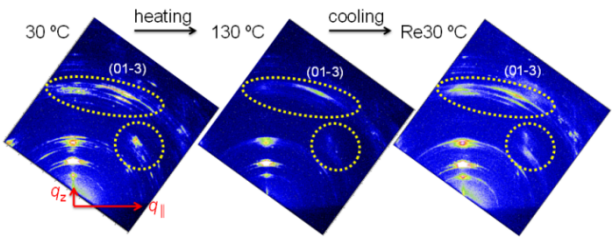

Fig. 6 2D GIWAXS patterns of the thinner film (~3 μm) of [F·DB24C8](PF$_6$) at 30 °C, 130 °C and after being cooled under ambient conditions to 30 °C.

To better understand the temperature-modulated flip-flop switch of the molecular alignments in the LT–HT phase transitions of the pseudorotaxane film, we prepared GIWAXS profiles from the in situ 2D GIWAXS images along the q_z direction, i.e. the {01−1} plane, and (01−3) plane for the as-cast pseudorotaxane film. The film annealed at 130 °C and cooled to 30 °C after being annealed (Fig. 7). Notably, the GIWAXS patterns taken at a grazing incident angle could not reveal crystalline structures in a truly vertical orientation with respect to the film surface[21] because of a missing diffraction zone in the corresponding pole figure illustrated in Fig. 7a (which was converted from the measured GIWAXS pattern in Fig. 5).[21] Nevertheless, in the analysis below, we use the GISAXS profiles taken along the nominal q_z direction for comparison. As revealed by the GIWAXS profiles in Fig. 7b, the crystalline layer thickness, i.e. the *d*-spacing along the {01−1} planes, shrank from 20.11 Å (q = 0.312 Å^{-1}) in the crystalline phase to 18.48 Å (q = 0.340 Å^{-1}) in the HT crystal phase for a more tightly intercalated crystal structure. Because the crystalline phase of the as-cast film is a solvent-assisted metastable phase, such a thermally induced structural transition is irreversible. Nevertheless, largely overlapped GIWAXS profiles taken at 130 °C and at 30 °C along the q_z direction in Fig. 7b returned, indicating that the solvent-induced clathrate structure could facilitate both the shrinkage of layers along q_z and subsequent reversible LT–HT phase transitions.

Although the basic frame structure is stable in these structural transitions, subtle structural transitions can be identified by the evolution of the reflections in the off-normal direction. Fig. 7c shows the selected intensity profiles extracted from the temperature-dependent 2D GIWAXS patterns shown in Fig. 6 along the {01−3} plane for the thin film of pseudorotaxane. The representative peaks (01−3), (020) and (002) are thermally reversible between 30 and 130 ºC. Among them, the thermally reversible structural transitions along the {01−3} plane are identical to that shown in the schematic in Fig. 3c. Specifically, in the HT crystalline phase at 130 °C, ordering peaks along this {01−3} were substantially suppressed, indicating deteriorated local ordering (of axle molecules) in this direction. Nevertheless, the layered structure was largely maintained, as indicated by the stable peaks along the {01−1} plane (Fig. 7b). Under close scrutiny, a shift of the (01−3) peak from q = 1.18 Å^{-1} in the case of the LT crystalline phase to 1.19 Å^{-1} in the case of the HT phase reveals a tightened *d*-spacing along (01−3) in the LT–HT phase transition (Fig. 7c).

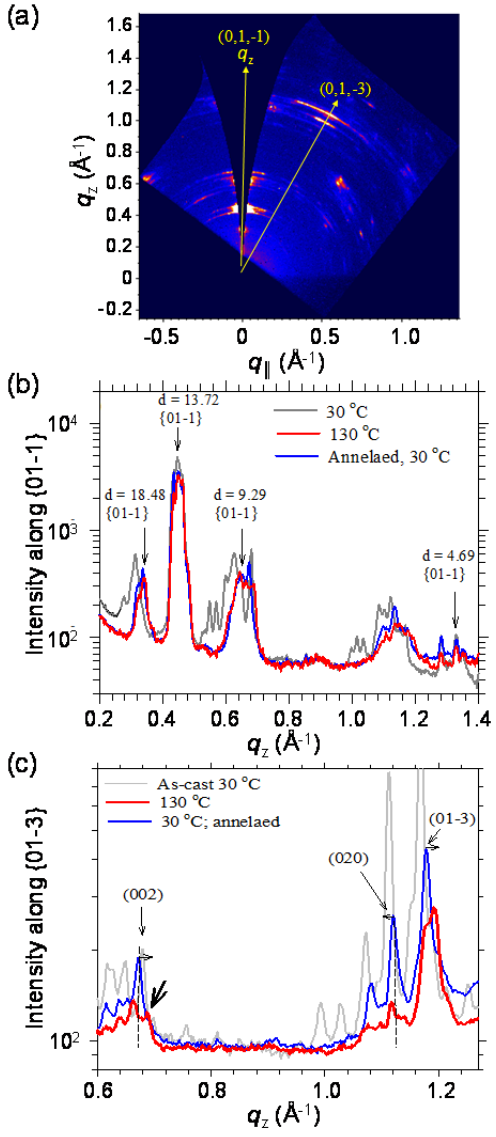

Fig. 7 (a) A pole figure converted from the GIWAXS pattern shown in Fig. 5. (b) GIWAXS profiles taken from the in situ 2D GIWAXS images along the nominal q_z direction, i.e. the {01−1} plane, for the as-cast pseudorotaxane film and for the film annealed at 130 °C and 30 °C after annealing. The arrows mark the {01−1} peaks that shifted during the

transition from the LC phase (as-cast) to a HT crystal phase (130 °C) and then to a LT crystal phase (30 °C). (c) Corresponding temperature-dependent GIWAXS profiles along {01−3}.

The shortened *d*-spacing favours π–π interactions of the axle molecules of pseudorotaxane. Consequently, an additional peak could form at q = 0.686 Å^{-1} in the case of the HT phase (compared with the corresponding 0.67 Å^{-1} peak in the case of the LT phase), corresponding to a different packing behaviour of the axle molecules (via π–π stacking) in the (002) direction. Accompanying the appearance of this additional peak is the shift of the (020) peak at q = 1.12 Å^{-1} in the case of the LT phase to 1.11 Å^{-1} in the case of the HT phase (Fig. 7c). This shift reveals a dimensional expansion along the *b* lattice direction in the HT phase because of the relaxed packing (or expansion) of the ring molecules in this direction (cf. Fig. 3c). These collective, local and thermally reversible structural changes observed with GIWAXS coincide with the X-ray crystallographic results for bulk crystals and with the POM results previously illustrated for thin-film crystals.

On the basis of the results of the POM and GIWAXS analysis, a plausible mechanism for the film-forming process for the self-assembly of the supermolecules and subsequent phase transitions in thin films can be described by the three-stage process shown in Fig. 8. In Stage 1, sheet-like packing of pseudorotaxane could form via intramolecular and intermolecular (π–π) interactions in the chloroform solution, as illustrated in the diagram in Fig. 8. During solvent evaporation, these sheet-like crystal nuclides deposit on the substrate with the sheet planes preferentially aligned to the substrate surface for a layering structure; which serves as the basis of formation of a discotic columnar crystal phase upon solvent evaporation. In Stage 2, with high temperature annealing (130 °C), the solvent-assisted crystalline phase of the pseudorotaxane film transforms to a HT crystalline phase of a crystalline structure, with a substantially tightened layer structure and weakened association between the axle molecules. In Stage 3, a decrease in the temperature required for reduced thermal fluctuations markedly enhances association between the axle molecules, which leads to the structural transition from the HT phase to the LT phase; this HT–LT phase transition is a reversible process modulated by thermal energy.

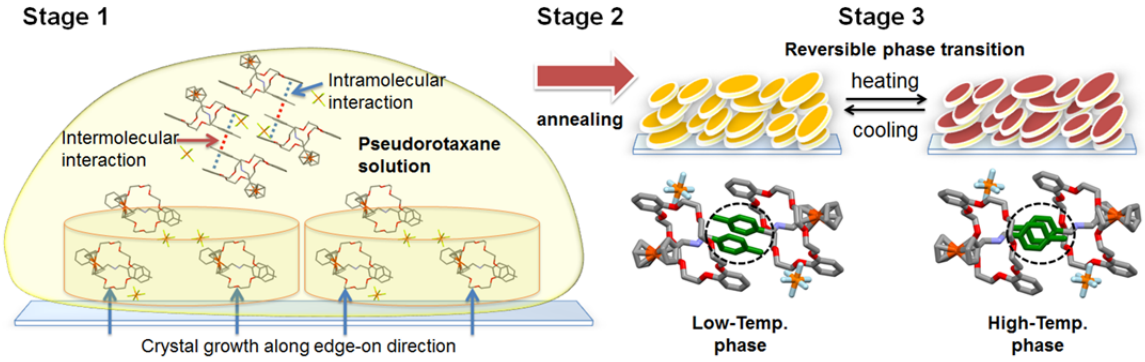

Fig. 8 Schematic of the formation of the pseudorotaxane film comprising highly oriented domains of a columnar LC phase. The phase transition originates from the thermally modulated competition between the ordering of the ring molecules and the ordering of the axle molecules, which leads to the changes in optical properties.

Conclusions

We have demonstrated the preparation and structural features of solution-cast films of pseudorotaxane. Because of the molecular interpenetration character of pseudorotaxane, balanced interactions within and in-between the host and guest molecules of the supermolecular complex as well as solvent evaporation during casting are critical parameters in forming the pseudorotaxane films that comprise highly oriented crystalline domains of poly-complexation structures on a solid substrate. The triclinic crystalline domain structure of the pseudorotaxane film matches well with that revealed by XRD and DSC for the corresponding large pseudorotaxane [F·DB24C8](PF_6) crystals, which confirms the complexation and crystallite structures of pseudorotaxane in the solution-cast and annealed films. As revealed by GIWAXS, the pseudorotaxane molecules in the film can be highly oriented with respect to the film normal direction. Therein, the cyclic host molecules adopt an edge-on orientation, with one side of the oligo-ethylene glycol group $(CH_2CH_2O)_n$ of the DB24C8 of the pseudorotaxane film anchoring to the substrate, resulting in a molecular plane perpendicular to the substrate surface. Supermolecular plate-like aggregates of the complex of the cyclic host and bulky guest axle molecules, serve as the building blocks for formation of the discotic columnar crystalline phase; transition of the crystalline phase to the thermally reversible crystalline phases can be induced at a moderate temperature of ~130 °C. The collective, local and thermally reversible structural changes observed by GIWAXS and POM provide a blueprint for the self-assembly of pseudorotaxane films with a thermally modulated stimulus response.

Acknowledgements

The authors thank the National Science Council of Taiwan for financial support.

References

1 *(a)* J. D. Badjic, V. Balzani, A. Credi, S. Silvi, J. F. Stoddart, *Science.*, 2004, **303**, 1845; *(b)* Coskun, A. Banaszak, M., Astumian, R. D., Stoddart, J. F. & Grzybowski, B. A. *Chem. Soc. Rev.*, 2012, **41**, 19.

2 A. Carlone, S. M. Goldup, N. Lebrasseur, D. A. Leigh, A. Wilson, *J. Am. Chem. Soc.*, 2012, **134**, 8321.

3 Z. Zhu, A. C. Fahrenbach, H. Li, J.C. Barnes, Z. Liu, S. M. Dyar, H. Zhang, J, Lei, R.Carmieli, A. A. Sarjeant, C. L. Stern, M.R. Wasielewski, J. F. Stoddart, *J. Am. Chem. Soc.*, 2012, **134**, 11709.

4 C. H. Lu, A. Cecconello, J. Elbaz, A. Credi, I. Willner, *Nano Lett.*, 2013, **13**, 2303.

5 *(a)* Juluri, B. K.; Kumar, A. S.; Liu, Y.; Ye, T.; Yang, Y. W.; Flood, A. H.; Fang, L.; Stoddart, J. F.; Weiss, P. S.; Huang, T. J. *ACS Nano.*, 2009, **3**, 291; Zhang, W. Y.; DeIonno, E.; Dichtel, W. R.; Fang, L.; Trabolsi, A.; Olsen, J. C.; *(b)* Benitez, D.; Heath, J. R.; Stoddart, J. F. *J. Mater. Chem.*, 2011, **21**, 1487.

6 Berna, J.; Leigh, D. A.; Lubomska, M.; Mendoza, S. M.; Perez, E. M.; Rudolf, P.; Teobaldi, G.; Zerbetto, F. *Nat. Mater.*, 2005, **4**, 704.

7 *(a)* M. A. Garcia-Garibay, *Proc. Natl. Acad. Sci.*, 2005, **102**, 10771; *(b)* B. Rodriguez-Molina, N. Farfan, M. Romero, J. M. Mendez-Stivalet, R. Santillan, M. A. Garcia-Garibay, *J. Am. Chem. Soc.*, 2011, **133**,7280; *(c)* C. S. Vogelsberg, M. A. Garcia-Garibay, *Chem. Soc. Rev.*, 2012, **41**, 1892.

8 V. N. Vukotic, K. J. Harris, K. Zhu, R. W. Schurko, S. J. Loeb, *Nat. Chem.*, 2012, **4**, 456.

9 *(a)* Q. W. Li, W. Y.Zhang, O. S. Miljanic, C. H. Sue, Y. L. Zhao, L. H. Liu, C. B. Knobler, J. F. Stoddart, O. M. Yaghi, *Science.*, 2009, **325**, 855; *(b)* A. Coskun, M. Hmadeh, G. Barin, F. Gandara, Q. W. Li, E. Choi, N. L. Strutt, D. B. Cordes, A. M. Z. Slawin, J. F. Stoddart, J. P. Sauvage, O. M. Yaghi, *Angew. Chem., Int. Ed.*, 2012, **51**, 2160; *(c)* H. X. Deng, M. A. Olson, J. F. Stoddart, O. M. Yaghi, *Nat. Chem.*, 2010, **2**, 439.

10 G. De Luca, E. Treossi, A. Liscio, J. M. Mativetsky, L. M. Scolaro, V. Palermo, P. Samorì, *J. Mater. Chem.*, 2010, **20**, 2493.

11 A. Datar, R. Oitker, L. Zang, *Chem. Commun.*, 2006, **0**, 1649.

12 L. Zalewski, S. Brovelli, M. Bonini, J. M. Mativetsky, M. Wykes, E. Orgiu, T. Breiner, M. Kastler, F. Dötz, F. Meinardi, H. L. Anderson, D. Beljonne, F. Cacialli, P. Samorì, *Adv. Funct. Mater.*, 2011, **21**, 834.

13 H.Tanaka, T. Ikeda, M. Takeuchi, K. Sada, S. Shinkai, T. Kawai, *Acs Nano.*, 2011, **5**, 9575.

14 *(a)* M. Horie, Y. Suzaki, K. Osakada, *Inorg. Chem.*, 2005, **44**, 5844; *(b)* M. Horie, Y. Suzaki, K. Osakada, T. Sassa, D. Hashizume, T. Wada, *Angew. Chem., Int. Ed.*, 2007, **46**, 4983; *(c)* M. Horie, Y. Suzaki, D. Hashizume, T. Abe, T. Wu, T. Sassa, T. Hosokai, K. Osakada, *J. Am. Chem. Soc.*, 2012, **134**, 17932.

15 U. Jeng, C. H. Su, C. J. Su, K. F. Liao, W. T. Chuang, Y. H. Lai, J. W. Chang, Y. J. Chen, Y. S. Huang, M.-T. Lee, K.-L. Yu, J.-M. Lin, D.-G. Liu, et al. *J. Appli. Crystallo.*, 2010, **43**, 110.

16 N. Boucher, J. Leroy, S. Sergeyev, E. Pouzet, V. Lemaur, R. Lazzaroni, J. Cornil, Y. H. Geerts, M. Sferrazza, *Syn. Metals.*, 2009, **159**, 1319.

17 C. Meyer, L. L. Cunff, M. Belloul, G. Foyart, *Materials.*, 2009, **2**, 499.

18 W. Chen, M. P. Nikiforov, S. B. Darling, *Energy Environ. Sci.*, 2012, **5**, 8045.

19 Waters, H.; Kettle, J.; Chang, S.-W.; Su, C.-J.; Wu, W.-R.; Jeng, U.; Tsai, Y.-C.; Horie, M.; *J. Mater. Chem. A.*, 2013, **1**, 7370.

20 T. Hosokai, M. Horie, T. Aoki, S. Nagamatsu, S. Kera, K. K. Okudaira, N. Ueno, *J. Phys. Chem. C*, 2008, **112**, 4643.

21 J. L. Baker, L. H. Jimison, S. Mannsfeld, S. Volkman, S. Yin, V. Subramanian, A. Salleo, A. Paul Alivisatos, Michael F. Toney, *Langmuir*, 2010, **26**, 9146.